A Novel Linear Polarization Resistance Corrosion Sensing Methodology for Aircraft Structure

Douglas W. Brown[1], Richard J. Connolly[2], Bernard Laskowski[3], Margaret Garvan[4], Honglei Li[5], Vinod S. Agarwala[6], and George Vachtsevanos[7]

[1,2,3] *Analatom, Inc., 3210 Scott Blvd., Santa Clara, CA 95054, USA*
doug.brown@analatom.com
richard.connolly@analatom.com
bernard.laskowski@analatom.com

[4,5,7] *Department of Electrical and Computer Engineering, Georgia Institute of Technology, Atlanta, GA 30332, USA*
mgarvan3@gatech.edu
honglei.li@gatech.edu
gjv@gatech.edu

[6] *Iron Pillar Technical Services, 1600 Green Street, Philadelphia, PA 19130, USA*
vsagarwala@comcast.net

ABSTRACT

A direct method of measuring corrosion on a structure using a micro-linear polarization resistance (μLPR) sensor is presented. The new three-electrode μLPR sensor design presented in this paper improves on existing LPR sensor technology by using the structure as part of the sensor system, allowing the sensor electrodes to be made from a corrosion resistant or inert metal. This is in contrast to a two-electrode μLPR sensor where the electrodes are made from the same material as the structure. A controlled experiment, conducted using an ASTM B117 salt fog, demonstrated the three-electrode μLPR sensors have a longer lifetime and better performance when compared to the two-electrode μLPR sensors. Following this evaluation, a controlled experiment using the ASTM G85 Annex 5 standard was performed to evaluate the accuracy and precision of the three-electrode μLPR sensor when placed between lap joint specimens made from AA7075-T6. The corrosion computed from the μLPR sensors agreed with the coupon mass loss to within a 95% confidence interval. Following the experiment, the surface morphology of each lap joint was determined using laser microscopy and stylus-based profilometry to obtain local and global surface images of the test panels. Image processing, feature extraction, and selection tools were then employed to identify the corrosion mechanism (e.g. pitting, intergranular).

1. INTRODUCTION

Recent studies have exposed the generally poor state of our nation's critical infrastructure that has resulted from wear and tear under excessive operational loads and environmental conditions. The British Standards Institution's Publicly Available Specification for the optimized management of physical assets defines asset management as the "systematic and coordinated activities and practices through which an organization optimally and sustainably manages its assets and asset systems, their associated performance, risks and expenditures over their life cycles for the purpose of achieving its organizational strategic plan." The motivation for effective asset management is driven by owners' desire for higher value assets at less overall costs, thus extracting the maximum value from their assets (Herder & Wijnia, 2011). Condition-based maintenance aims to maximize asset value by extending the useful life of assets through mitigation of unnecessary maintenance actions performed during schedule-based maintenance strategies (Huston, 2010). By providing maintenance engineers with information regarding the health of the structure, maintenance can be performed on a basis of necessity unique to each asset, as opposed to schedule-based predictions formed on statistical trends of operational reliability. These systems must be low-cost and simple to install with a user interface designed to be easy to operate.

To reduce the cost and complexity of such a system for monitoring corrosion in an avionics environment, a generic interface node using low-powered wireless communications has

Figure 1. AN110 installed on a C-130H

been developed. This node can communicate with a myriad of common sensors used in SHM. In this manner a structure such as a bridge, aircraft, or ship can be fitted with sensors in any desired or designated location and format without the need for communications and power lines that are inherently expensive and complex to route. Data from these nodes is transmitted to a central communications personal computer for data analysis. An example of this is provided in Figure 1 showing an embedded AN110 SHM system installed on a C-130H aircraft.

The micro-linear polarization resistance (μLPR) sensor presented in this paper improves on existing LPR technology by using the structure as part of the sensing system. The sensor includes three electrodes, where each electrode is fabricated on a flexible substrate to create a circuit consisting of gold-plated copper. The first two electrodes, or the counter and reference electrodes, are configured in an interdigitated fashion with a separation distance of 8mil. The flex cable contains a porous membrane between the pair of electrodes and the structure. A third electrode, or the working electrode makes electrical contact to the structure through a 1mil thick electrically conductive transfer tape placed between the electrode and structure. The reference and counter electrodes are electrically isolated from the working electrode and physically separated from the surface of the structure by 1mil. The flex cable can be attached to the structure with adhesives or in the case of placement in a butt joint or lap joint configuration, by the mechanical forces present in the joint itself. Corrosion is computed from known physical constants, by measuring the polarization resistance between the electrolytic solution and the structure. Further improvements are realized by narrow-

ing the separation distance between electrodes, which minimizes the effects due to solution resistance. This enables the μLPR to operate more effectively outside a controlled aqueous environment, such as an electrochemical cell, in a broad range of applications (eg. civil engineering, aerospace, petrochemical).

The remainder of the paper is organized as follows. Section 2 provides background information on different corrosion sensing technologies, LPR theory, and the new 3-electrode μLPR sensor design. Section 3 describes the experimental procedure used to evaluate the new sensor design through a controlled ASTM G85 Annex 5 cyclic salt fog test. Section 4 presents the results of experimental testing comparing the corrosion rate computed from μLPR sensor data with measured mass loss. Also presented are correlations between features, exposure time, and μLPR sensor measurements. Finally, the paper is concluded in Section 5 with a summary of the findings and future work.

2. BACKGROUND

Corrosion sensors can be distinguished by the following categories, *direct* or *indirect* and *intrusive* or *non-intrusive*. Direct corrosion monitoring measures a response signal, such as a current or potential, resulting from corrosion. Examples of common direct corrosion monitoring techniques are: corrosion coupons, electrical resistance (ER), electrochemical impedance spectroscopy (EIS), and linear polarization resistance (LPR) techniques. Whereas, indirect corrosion monitoring techniques measure an outcome of the corrosion process. Two of the most common indirect techniques are ultrasonic testing and radiography. An intrusive measurement requires access to the structure. Corrosion coupons, ER, EIS, and LPR probes are intrusive since they have to access the structure. Non-intrusive techniques include ultrasonic testing and radiography.

Each of these methods have advantages and disadvantages. Corrosion coupons provide the most reliable physical evidence possible. Unfortunately, coupons usually require significant time in terms of labor and provide time averaged data that can not be utilized for real-time or on-line corrosion monitoring (Harris, Mishon, & Hebbron, 2006). ER probes provide a basic measurement of metal loss, but unlike coupons, the value of metal loss can be measured at any time, as frequently as required, while the probe is *in situ* and permanently exposed to the structure. The disadvantage is ER probes require calibration with material properties of the structure to be monitored. The advantage of the LPR technique is that the measurement of corrosion rate is made instantaneously. This is a more powerful tool than either coupons or ER where the fundamental measurement is metal loss and some period of exposure is required to determine corrosion rate. The disadvantage to the LPR technique is that it can only be suc-

cessfully performed in relatively clean aqueous electrolytic environments (*Introduction to Corrosion Monitoring*, 2012). EIS is a very powerful technique that can provide a corrosion rate and classification of the corrosion mechanism. EIS measures the magnitude and phase response of an electrochemical cell. Physical parameters, such as the polarization resistance, solution resistance, and double-layer capacitance, can be derived from these responses, which provides more information than just LPR alone. The disadvantage with EIS is that it uses sophisticated instrumentation that requires a controlled setting to obtain an accurate spectrum. In fielded environments, EIS is highly susceptible to noise. Additionally, interpretation of the data can be difficult (Buchheit, Hinkebein, Maestas, & Montes, 1998). Ultrasonic testing and radiography can be used to detect and measure (depth) corrosion through non-destructive and non-intrusive means (Twomey, 1997). The disadvantage with the ultrasonic testing and radiography equipment is the same with corrosion coupons, both require significant time in terms of labor and can not be utilized for real-time or on-line corrosion monitoring. As this paper is focused on a three-electrode μLPR sensor, the remainder of the background will focus on LPR.

2.1. LPR Theory

Corrosion occurs as a result of oxidation and reduction reactions occurring at the interface of a metal and an electrolyte solution. This process occurs by electrochemical half-reactions; (1) anodic (oxidation) reactions involving dissolution of metals in the electrolyte and release of electrons, and (2) cathodic (reduction) reactions involving gain of electrons by the electrolyte species like atmospheric oxygen, O_2, H_2O, or H^+ ions in an acid (Harris et al., 2006). The flow of electrons from the anodic reaction sites to the cathodic reaction sites creates a corrosion current. The electrochemically generated corrosion current can be very small (on the order of nanoamperes) and difficult to measure directly. Application of an external potential exponentially increases the anodic and cathodic currents, which allows instantaneous corrosion rates to be extracted from the polarization curve. Extrapolation of these polarization curves to their linear region provides an indirect measure of the corrosion current, which is then used to calculate the rate of corrosion (Burstein, 2005).
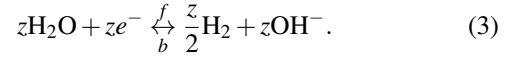
The electrochemical technique of LPR is used to study corrosion processes since the corrosion reactions are electrochemical reactions occurring on the metal surface. Modern corrosion studies are based on the concept of mixed potential theory postulated by Wagner and Traud, which states that the net corrosion reaction is the sum of independently occurring oxidation and reduction reactions (Wagner & Traud, 1938). For the case of metallic corrosion in presence of an aqueous medium, the corrosion process can be written as,

$$M + zH_2O \underset{b}{\overset{f}{\leftrightarrow}} M^{z+} + \frac{z}{2}H_2 + zOH^-, \qquad (1)$$
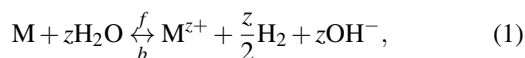
where z is the number of electrons lost per atom of the metal. This reaction is the result of an anodic (oxidation) reaction,

$$M \underset{b}{\overset{f}{\leftrightarrow}} M^{z+} + ze^-, \qquad (2)$$

and a cathodic (reduction) reaction,

$$zH_2O + ze^- \underset{b}{\overset{f}{\leftrightarrow}} \frac{z}{2}H_2 + zOH^-. \qquad (3)$$

It is assumed that the anodic and cathodic reactions occur at a number of sites on a metal surface and that these sites change in a dynamic statistical distribution with respect to location and time (Kossowsky, 1989). Thus, during corrosion of a metal surface, metal ions are formed at anodic sites with the loss of electrons and these electrons are then consumed by water molecules to form hydrogen molecules. The interaction between the anodic and cathodic sites as described on the basis of mixed potential theory is represented by well-known relationships using current (reaction rate) and potential (driving force). For the above pair of electrochemical reactions (2) and (3), the relationship between the applied current I_a and applied potential, E_a, follows the Butler-Volmer equation,

$$I_a = I_{corr}\left[e^{2.303(E_a - E_{corr})/\beta_a} - e^{-2.303(E_a - E_{corr})/\beta_c}\right], \qquad (4)$$

where β_a and β_c are the anodic and cathodic Tafel parameters given by the slopes of the polarization curves $\partial E_a/\partial \log_{10} I_a$ in the anodic and cathodic Tafel regimes, respectively and E_{corr} is the corrosion, or open circuit potential (Bockris, Reddy, & Gambola-Aldeco, 2000). The corrosion current, I_{corr}, cannot be measured directly. However, *a priori* knowledge of β_a and β_c along with a small signal analysis technique, known as polarization resistance, can be used to indirectly compute I_{corr}. The polarization resistance technique, also referred to as linear polarization, is an experimental electrochemical technique that estimates the small signal changes in I_a when E_a is perturbed by $E_{corr} \pm 10$mV (G102, 1994). The slope of the resulting curve over this range is the polarization resistance,

$$R_p \triangleq \left.\frac{\partial E_a}{\partial I_a}\right|_{|E_a - E_{corr}| \leq 10\text{mV}}. \qquad (5)$$

ASTM standard G59 outlines procedures for measuring polarization resistance. Potentiodynamic, potential step, and current-step methods can be used to compute R_p (G59, 1994). The potentiodynamic sweep method is the most common method for measuring R_p. A potentiodynamic sweep is conducted by applying E_a between $E_{corr} \pm 10$mV at a slow scan rate, typically $0.125\,\text{mV/s}$. A linear fit of the resulting E_a vs. I_a curve is used to compute R_p. Note, the applied current, I_a, is the total applied current and is not multiplied by the electrode area so R_p as defined in (5) has units of Ω. Provided that $|E_a - E_{corr}|/\beta_a \ll 1$ and $|E_a - E_{corr}|/\beta_c \ll 1$, the first order
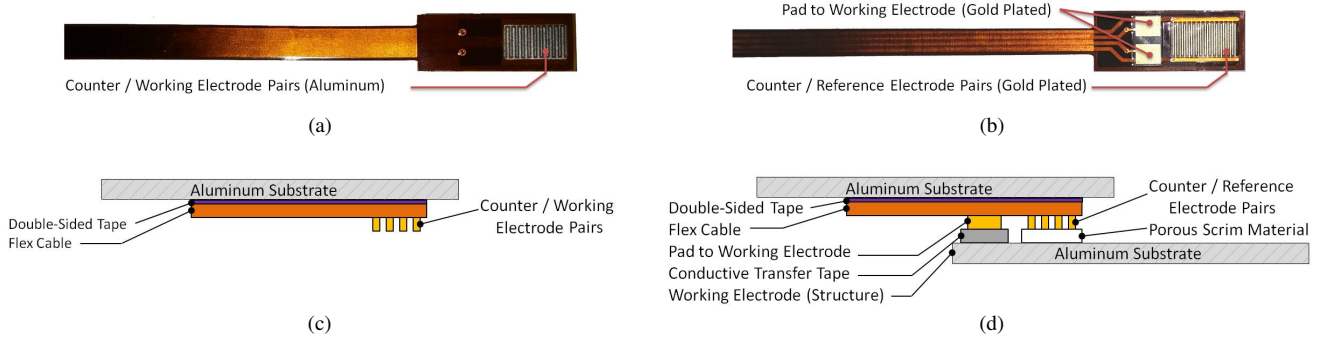
Figure 2. The (a) two-electrode μLPR sensor, (b) three-electrode μLPR sensor, (c) two-electrode μLPR sensor identifying each sensor element when mounted to a substrate, and (d) three-electrode μLPR sensor identifying each sensor element when attached using the structure as the third electrode.

Taylor series expansion $e^x \approx 1 + x$ can be applied to (4) and (5) to arrive at the Stern-Geary equation,

$$I_{corr} = \frac{B^\star}{R_p}, \tag{6}$$

where,

$$B^\star = \frac{\beta_a \beta_c}{2.303 \, (\beta_a + \beta_c)}. \tag{7}$$

Knowledge of R_p, β_a, and β_c enables direct determination of I_{corr} at any instant in time. The corrosion rate, R_{loss}, can be found by applying Faraday's law,

$$R_{loss}(t) = \frac{B_{loss}}{R_p(t)}, \tag{8}$$

where,

$$B_{loss} = \frac{B^\star}{FA_{sen}} \left(\frac{AW}{z} \right), \tag{9}$$

such that F is Faraday's constant, z is the number of electrons lost per atom of the metal during an oxidation reaction, A_{sen} is the effective area of the sensor, and AW is atomic weight. The total mass loss, M_{loss}, due to corrosion can be found by integrating (8),

$$M_{loss}(t) = \int_{t_0}^{t} R_{loss}(\tau) \, d\tau. \tag{10}$$

Finally, since R_p is not measured continuously (10) needs to be discretized for the sample period T_s,

$$M_{loss}(t) \Big|_{t=NT_s} = T_s \sum_{k=1}^{N} R_{loss}(kT_s). \tag{11}$$

2.2. Sensor Design

The two-electrode μLPR design consists of a sensor with interdigitated electrodes photo-etched from 2 mil aluminum shim-stock material with a thickness and separation distance

of 12 mil. In this configuration one of the electrode pairs acts as the counter electrode (cathode) and the other as the working electrode (anode). The sensor is designed to corrode in the same environment as the structure, effectively measuring the corrosivity of the environment. An image of the two-electrode μLPR sensor is provided in Figure 2(a). An illustration showing the two-electrode μLPR sensor mounted to the structure is shown in Figure 2(c).

Improving on the two-electrode design, the three-electrode μLPR is fabricated on a flexible Kapton substrate where each electrode is coated with a noble metal. The first two electrodes, counter and reference electrodes, are fabricated using 0.5 oz. copper with an electroless nickel immersion gold (ENIG) finish and an overall thickness of 1 mil. The counter and reference electrode pair is configured in a interdigitated geometric layout with a separation distance of 9 mil. The flex cable contains an insulating porous scrim material between the pair of electrodes and the structure. A third electrode, made from the same ENIG finish, is placed in close proximity to the counter and reference electrodes; electrical contact is made with the structure by placing a 1 mil thick electrically conductive transfer tape between the electrode and structure. This allows the structure to serve as the working electrode for the sensor measurement. The flex cable, shown in Figures 2(b) and (d), can be attached to the structure through the use of adhesives or in the case of placement in a butt joint or lap joint configuration, the holding force is provided by the joint itself.

3. EXPERIMENTAL PROCEDURES

3.1. Tafel Measurements

ASTM standard G59 outlines the procedure for measuring the Tafel slopes, β_a and β_c. First, E_{corr} is measured from the open circuit potential. Next, E_a is initialized to E-corr-250mV. Then, a potentiodynamic sweep is conducted by increasing E_a from $E_{corr} - 250$mV to $E_{corr} + 250$mV at a slow
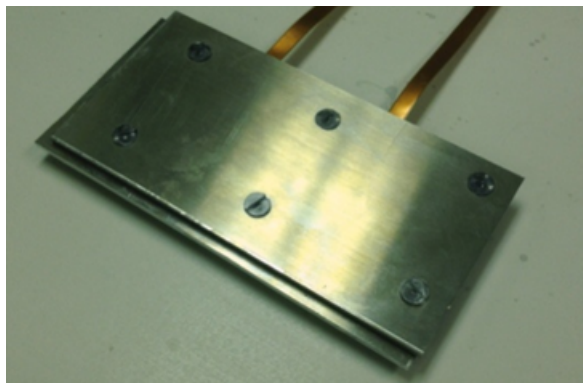
Figure 3. AA7075-T6 lap joint assembly.

Figure 4. Panels shown in the corrosion chamber prior to the experiment.

scan rate, typically $0.125\,\mathrm{mV/s}$. Finally, a Tafel curve is plotted for E_a vs. $\log_{10} I_a$. Values for β_a and β_c are estimated from the slopes of the linear extrapolated anodic and cathodic currents.

3.2. Sample Preparation

Lap joint samples were made using two 6" by 3" panels made from AA7075-T6 with a thickness of 1/8". These panels were secured together with six polycarbonate fasteners. Before assembly of the lap joint each panel was cleaned with a 35 min immersion into a constantly stirred solution of $50\,\mathrm{g/L}$ Turco 4215 NC-LT at $65°$C. After completing this alkaline cleaning the panels were rinsed with deionized water and immersed into a 70% solution of nitric acid solution for 5 min at $25°$C. The samples were then rinsed again in the deionized water and air dried. Weights were recorded to the nearest fifth significant figure and the samples were stored in a desiccator. Once the panels were prepared and massed, two μLPR sensors were installed between the panels. At this point the six polycarbonate bolts were torqued down evenly to $2\,\mathrm{N\cdot m}$. This lap joint assembly is shown in Figure 3. After assembling the lap joints, the samples were evenly coated with 2 mils of epoxy-based paint and 2 mils of polyurethane on all exposed surfaces. These coatings were allowed to fully seal over a 24 hour period at $35°$C before testing.

3.3. Comparing Two vs. Three Electrode Design

A preliminary experiment was performed to highlight the benefits between a two-electrode μLPR sensor made from AA7075-T6 and a three-electrode μLPR sensor made from nickel. This experiment was performed by placing four two-electrode μLPR and four three electrode μLPR sensors into a beaker filled with a B117 salt solution modified to a pH of 5.5. A stirbar was used to constantly mix the solution. The sensors were placed inside the beaker around a plastic cylindrical fixture. The two and three-electrode μLPR sensors were evenly spaced in an alternating arrangement. Approximately every 4 days, the coupons were removed, cleaned, massed and then
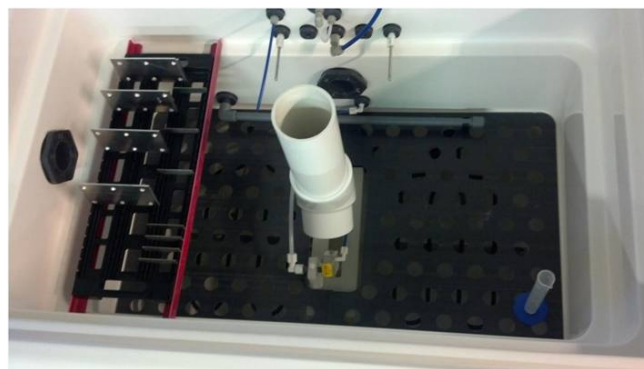
returned to the beaker to resume the experiment.

3.4. Accelerated Lap Joint Testing

Corrosion tests were performed in a cyclic corrosion chamber running the ASTM G85 Annex 5 test. This test consisted of two one-hour steps. The first step involved exposing the samples to a salt fog for a period of one-hour at $25°$C. The electrolyte solution composing the fog was 0.05% sodium chloride and 0.35% ammonium sulfate in deionized water. This step was followed by a dry-off step, where the fog was purged from the chamber while the internal environment was heated to $35°$C. Each panel was positioned at a $60°$ angle with the flex tape facing downward, as not to allow a direct pathway for condensate to travel into the lap joints. Electrical connections for the μLPR sensors were made to an AN110 positioned outside the chamber by passing extension cables through a bulkhead. Temperature, relative humidity, and μLPR data were acquired at 1 min intervals.

3.5. Sample Cleaning

Samples were removed from the environmental chamber and disassembled. Following disassembly, the polyurethane and epoxy coatings on the aluminum panels were removed by placing them in a solution of methyl ethyl ketone. After immersion for 30 min the panels were removed and rinsed with deionized water. These panels were again alkaline cleaned with a 35 min immersion into a constantly stirred solution of $50\,\mathrm{g/L}$ Turco 4215 NC-LT at $65°$C. This was followed by a deionized water rinse and immersion into a $90°$C solution of 4.25% phosphoric acid containing $20\,\mathrm{g/L}$ chromium trioxide for 10 min. Following the phosphoric acid treatment, panels were rinsed with deionized water and placed into a 70% nitric acid solution for 5 min at $25°$C. Panels were then rinsed with deionized water, dipped in ethanol, and dried with a heat gun. This cleaning process was repeated until mass values for the panels stabilized. These values were then compared with mass loss values calculated from the μLPR data.

4. RESULTS

4.1. Comparing Two vs. Three Electrode Design

The Tafel constants were acquired while the panels were undergoing a wetting cycle. The Tafel constants were acquired and plotted as applied voltage vs. the logarithm of applied current magnitude, shown in Figure 5. From this plot the Tafel constants were computed as, $\beta_a = 0.40\,V/\text{dec}$ and $\beta_c = 0.15\,V/\text{dec}$. The corrosion constant, B_{loss}, was computed using (9) with the material properties for AA7075-T6 and sensor properties defined in the nomenclature. Note, the Tafel slope is an intensive parameter and does not depend on the electrode surface area. If the Tafel constants cannot be extrapolated, is not uncommon to approximate β_a and $\beta_c \approx 0.15\,V/\text{dec}$.

The total corrosion for each sensor was computed by applying (10) to integrate the corrosion rate with respect to time. For the first 300 hours of the experiment, both sensors produce comparable results. However, at 300 hours the overall LPR reading began to drop and the variance between sensor readings started to increase, as shown in Figures 6(a) and (b). This may result from a reduction in the effective surface area of the electrodes as a result of the corrosion process. As more corrosion begins to accumulate, the fingers become less and less effective. In contrast, the 95% confidence band for the three-electrode μLPR sensor remained relatively constant throughout the experiment, shown in Figure 6(c) and (d).

4.2. Lap Joint Testing Results

After selecting the three electrode μLPR for further evaluation, a set of four lap joints were assembled. These assemblies were tested over a maximum period of 286 hours, where the environment inside the chamber was cyclically varied in temperature and humidity according to ASTM G85 Annex 5 to promote corrosion. Panels were removed at 133, 209, 286, and 286 hours into the experiment, respectively. Plots of the measured temperature and humidity vs. time are provided in Figure 8. The corrosion rate, shown in Figure 7, was computed from R_p measurements using (8) along with B_{loss} computed during the previous experiment. The total corrosion, shown in Figure 9(a), was computed for each panel by applying (10) to integrate the corrosion rate with respect to time. The error bars correspond to the standard deviation observed at the time when the mass loss was computed. Finally, the measured and computed corrosion from the μLPR measurements were compared in a scatter plot, shown in Figure 9(b). The error bars in the y-direction correspond to observation error. These results indicate the measured corrosion correlated with the computed corrosion to within 95% confidence (two standard deviations of the observation error).

4.3. Lap Joint Imaging Feature

Microscopic images were acquired over a field size of $37\,\text{mm} \times 37\,\text{mm}$ at a magnification of 108x using the LEXT OLS4000 3D Laser Measuring Microscope. Comprehensive images of each panel was created by stitching together adjacent images. The rivet holes and numbers were manually changed to be white so they wouldn't be confused with corroded regions. To get the features a 2D median filter was applied followed by thresholding (using a threshold of 0.2) to get a binary image. The area for each object (each black region is considered to be an object) in the binary image was calculated. The sum of objects with an area larger than 50 pixels (this was to avoid counting dark regions caused by the grain boundaries as pits) was taken to be the area of the corroded region. The percent area of the corrosion was calculated as,

$$P_{area} = 100\% \cdot \frac{A_{corr}}{A_{image} - A_{rivets}}, \tag{12}$$

where A_{corr} is the area of the corroded region, A_{image} is the area of the image, and A_{rivets} is the area of the rivets. Figure 11 shows the original images of each panel along with a binary image for the specimens removed 133 hours, 209 hours and 286 hours into the experiment. Figure 10 shows plots of (a) P_{area} vs. time and (b) P_{area} vs. computed corrosion.

5. CONCLUSION

A new μLPR sensor design was presented for direct corrosion monitoring in structural health management (SHM) applications. The new design improves on existing technologies by: (1) using the structure as part of the sensor measurement; (2) improving sensor lifetime by making the electrodes from a non-corrosive material; and (3) improving on sensor performance by reducing the separation distance between the working, reference, and counter electrodes. Corrosion tests were performed in a cyclic corrosion chamber running ASTM G85-A5 salt fog test. The results indicate the μLPR sensor data correlated with the measured mass loss to within 95% confidence (two standard deviations of the observation error). This demonstrates the μLPR sensor can accurately measure the change in the corrosion rate as a function of time for a given electrolyte condition. Future work includes:

- Demonstrate μLPR sensor accurately measures the corrosion rate as a function of solution conductivity.

- Establish the μLPR sensor can accurately measure corrosion in atmospheric conditions where corrosion rates are lower than in an "accelerated corrosion chamber".

- Investigate the surface morphology of the coupons using a scanning electron microscope (SEM) and correlate the measured corrosion rate as a function of corrosion behavior as determined by the μLPR sensor data over time.
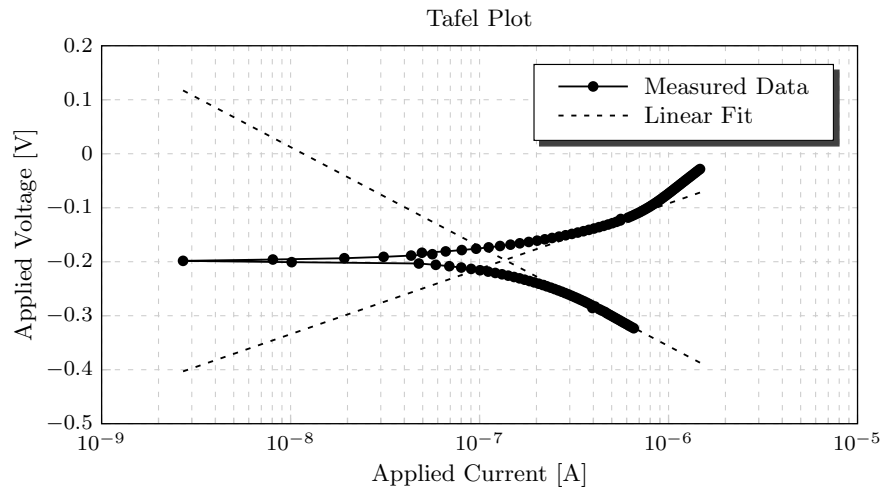
Figure 5. Tafel plot of the μLPR sensors.

(a)

(b)

(c)

(d)
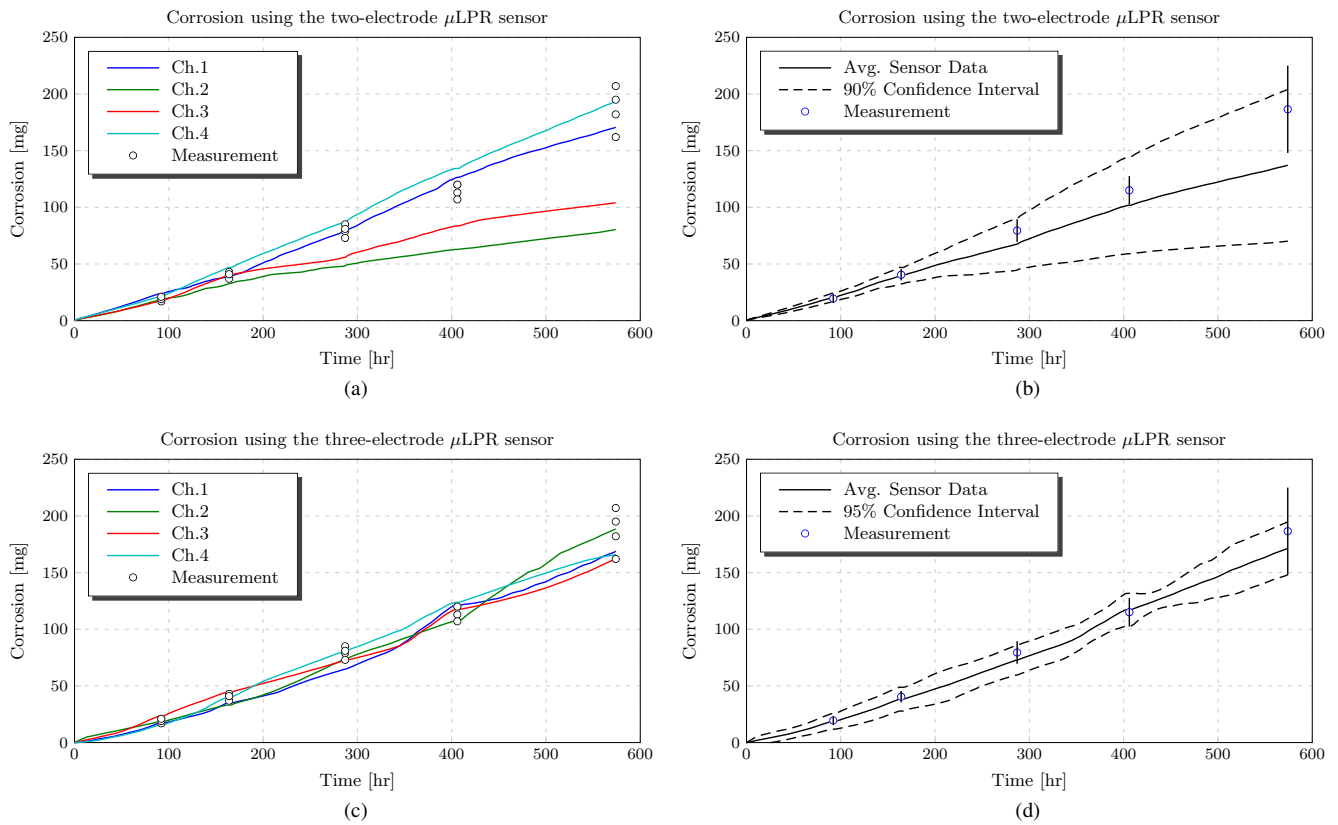
Figure 6. Corrosion vs. time for (a) four two-electrode μLPR sensor made from AA7075-T6, (b) the corresponding average with a 90% confidence interval, (c) corrosion vs. time for a three-electrode μLPR sensor made from nickel and (d) the corresponding average with a 95% confidence interval.
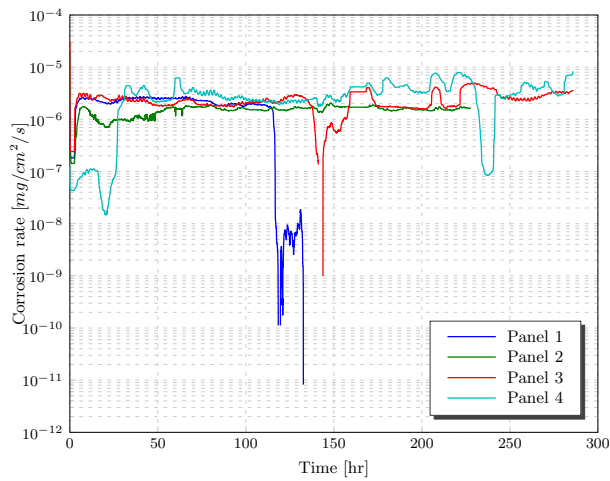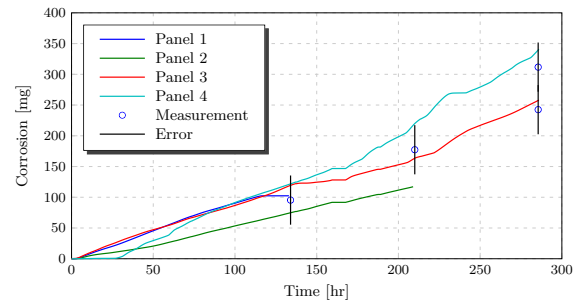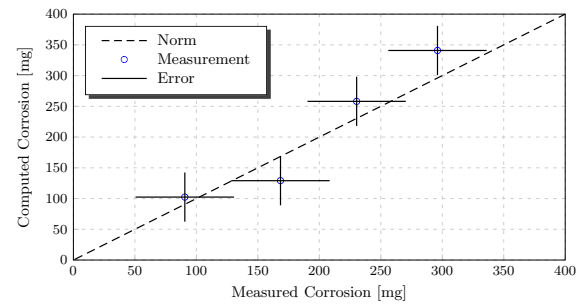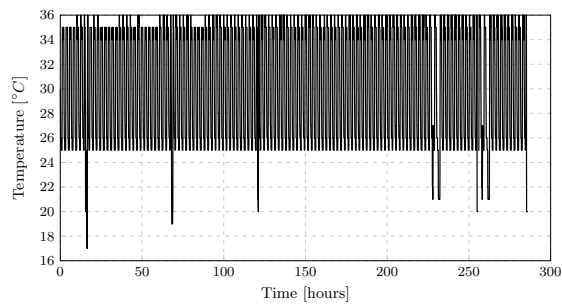
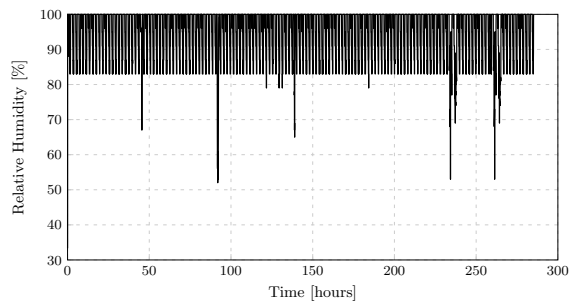Figure 7. Computed corrosion rate vs. time.

(a)

(b)

Figure 9. Plot of (a) computed corrosion vs. time and (b) measured vs. computed corrosion.
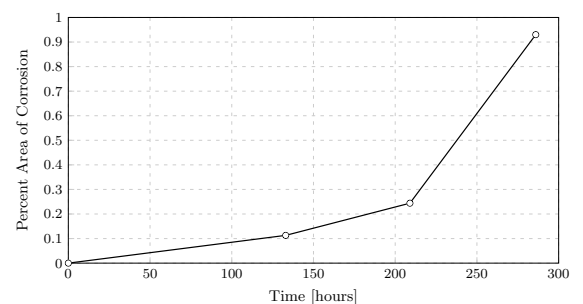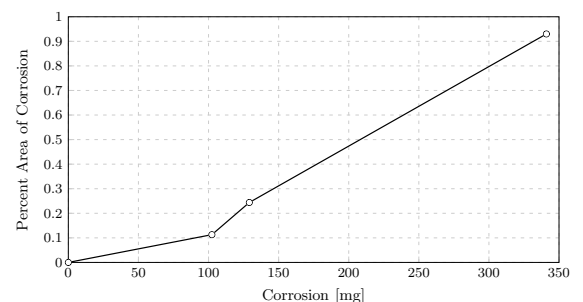

(a)

(b)

Figure 8. Plots of (a) temperature and (b) relative humidity vs. time.

(a)

(b)

Figure 10. Percent area of corrosion vs. (a) time and (b) computed corrosion.
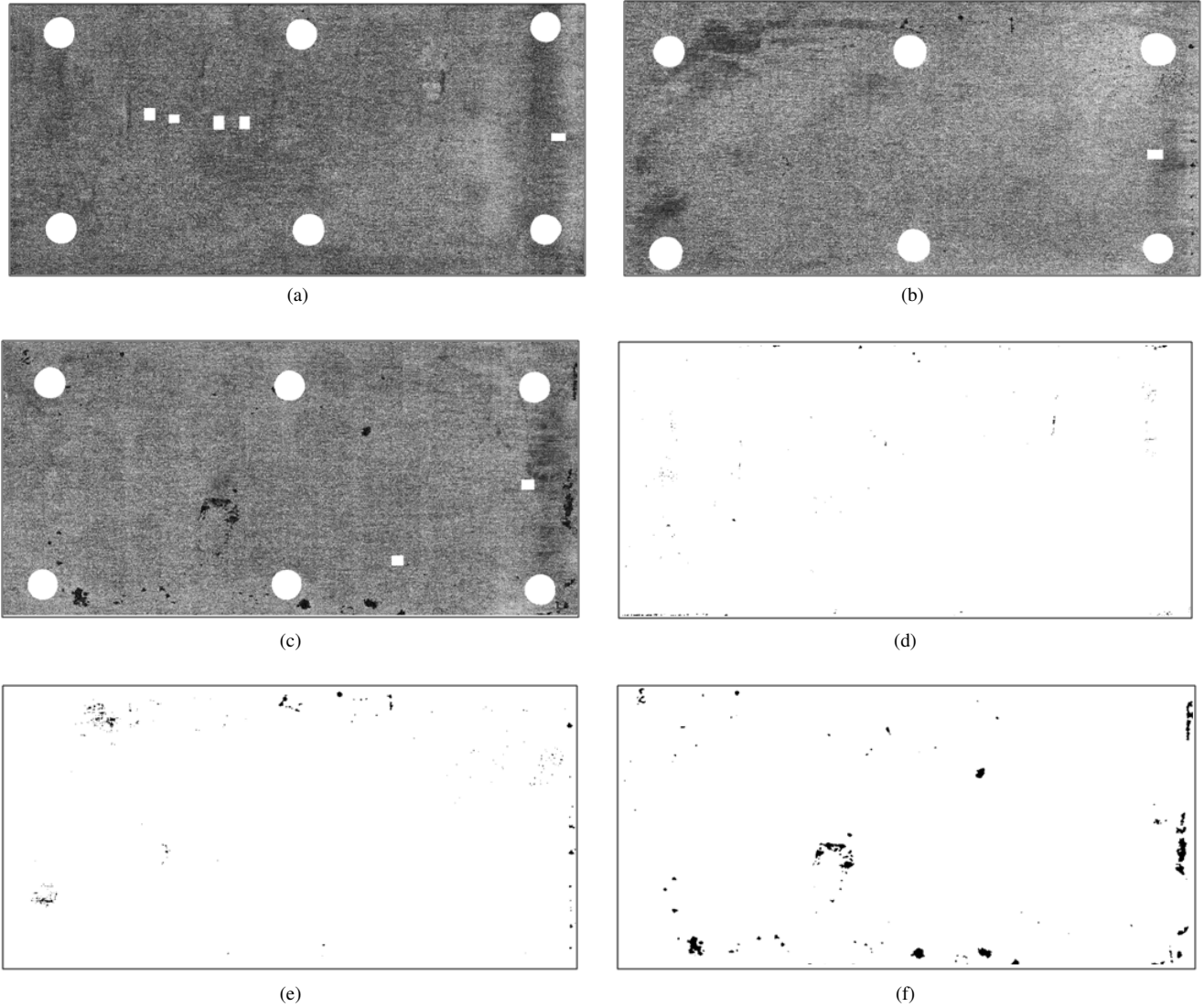
Figure 11. Original panel image with rivets and numbers removed for (a) 133 hours, (b) 209 hours, and (c) 286 hours of exposure time. Also shown is a binary image after filtering showing the percent area of corrosion for (d) 133 hours at 0.113%, (e) 209 hours at 0.244%, and (f) 286 hours at 0.93%.

NOMENCLATURE

β_a	V/dec	0.40	anodic Tafel constant
β_c	V/dec	0.15	cathodic Tafel constant
τ	s	-	time variable
$d\tau$	s	-	time step
k	-	-	sample index
t	s	-	time
t_0	s	-	initial time
z	-	3	electron loss
A_{corr}	cm^2	-	% area of corrosion
A_{image}	cm^2	-	% area of image
A_{rivets}	cm^2	-	% area of of rivets
A_{sen}	cm^2	4.233×10^{-2}	sensor area
AW	g/mol	2.899×10^1	atomic weight
$B^\star$	V/dec	4.95×10^{-2}	constant
B_{loss}	$\Omega \cdot$g/cm^2/s	1.170×10^{-4}	constant
E_a	V	-	applied potential
E_{corr}	V	-	corrosion potential
I_a	A/cm^2	-	applied current
I_{corr}	A/cm^2	-	corrosion current
F	C/mol	9.649×10^4	Faraday's constant
M_{loss}	g/cm^2	-	mass loss
N	-	-	total samples
P_{area}	-	-	Percent area of corrosion
R_{loss}	g/cm^2/s	-	corrosion rate
R_p	Ω	-	polarization resistance
T_s	s	60	sample period

REFERENCES

Bockris, J. O., Reddy, A. K. N., & Gambola-Aldeco, M. (2000). *Modern electrochemistry 2a. fundamentals of electrodics* (2nd ed.). New York: Kluwer Academic/Plenum Publishers.

Buchheit, R. G., Hinkebein, T., Maestas, L., & Montes, L. (1998, March 22-27). Corrosion monitoring of concrete-lined brine service pipelines using ac and dc electrochemical methods. In *Corrosion 98.* San Diego, Ca.

Burstein, G. T. (2005, December). A century of tafel's equation: 1905-2005. *Corrosion Science*, *47*(12), 2858-2870.

G102, A. S. (1994). Standard practice for calculation of corrosion rates and related information from electrochemical measurements. *Annual Book of ASTM Standards*, *03.02*.

G59, A. S. (1994). Standard practice for conducting potentiodynamic polarization resistance measurements. *Annual Book of ASTM Standards*, *03.02*.

Harris, S. J., Mishon, M., & Hebbron, M. (2006, October). Corrosion sensors to reduce aircraft maintenance. In *Rto avt-144 workshop on enhanced aircraft platform availability through advanced maintenance concepts and technologies.* Vilnius, Lithuania.

Herder, P., & Wijnia, Y. (2011). *Asset management: The state of the art in europe from a life cycle perspective* (T. van der Lei, Ed.). Springer.

Huston, D. (2010). *Structural sensing, health monitoring, and performance evaluation* (B. Jones & W. B. S. J. Jnr., Eds.). Taylor and Francis.

Introduction to corrosion monitoring. (2012, August 20). Online. Available from http://www.alspi.com/introduction.htm

Kossowsky, R. (1989). *Surface modification engineering* (Vol. 1). Boca Raton, Florida: CRC Press, Inc.

Twomey, M. (1997). Inspection techniques for detecting corrosion under insulation. *Material Evaluation*, *55*(2), 129-133.

Wagner, C., & Traud, W. (1938). *Elektrochem*, *44*, 391.

BIOGRAPHIES

Douglas W. Brown is the Senior Systems Engineer for Analatom, Inc. He received the bachelor of science degree in electrical engineering from the Rochester Institute of Technology and his master of science and doctor of philosophy degrees in electrical engineering from the Georgia Institute of Technology. Dr. Brown has ten years of experience developing and maturing Prognostics & Health Management (PHM) and fault-tolerant control systems in avionics application. He is a recipient of the National Defense Science and Engineering Graduate (NDSEG) Fellowship and has received several best-paper awards for his work in PHM and fault-tolerant control.

Richard J. Connolly is the Senior Research Engineer for Analatom, Inc. He completed his bachelor of science and doctor of philosophy degree in chemical and biomedical engineering at the University of South Florida. Dr. Connolly is

a fellow of the National Science Foundation and is regarded as an expert in interfacing of engineering devices with skin. He has extensive experience in bioelectrics, electrochemistry, and data analysis. Much of this experience was gained while performing bioelectric data collection on human and animal models. During his tenure at Analatom he has overseen testing and validation of the μLPR technology for aerospace and civil engineering applications.

Bernard Laskowski is the President and Senior Research Scientist at Analatom since 1981. He received the licentiaat and doctor of philosophy degrees in physics from the University of Brussels in 1969 and 1974, respectively. Dr. Laskowski has published over 30 papers in international refereed journals in the fields of micro-physics and micro-chemistry. As president of Analatom, Dr. Laskowski has managed 93 university, government, and private industry contracts, receiving a U.S. Small Business Administration Administrator's Award for Excellence.

Margaret Garvan received her master of science degree in electrical and computer engineering (ECE) from the Georgia Institute of Technology, and bachelor of science in electrical engineering from the University of Florida. She is currently a Ph.D. candidate and graduate research assistant at the Georgia Institute of Technology. Her research is focused on intelligent machine learning, and methodologies for diagnostics and prognostics for structural health monitoring.

Honglei Li received her master of science degree in electrical and computer engineering (ECE) from the Georgia Institute of Technology, and in Instrumental Engineering from Shanghai Jiao Tong University respectively. She is currently a graduate research assistant at Intelligent Control Systems Laboratory, working on her doctoral degree in ECE at the Georgia Institute of Technology. Her current research is focused on intelligent machine learning, methodologies for prognostics and structural health monitoring and health management, as well as asset life-cycle and risk management.

Vinod S. Agarwala Dr. Vinod S. Agarwala is a recently retired from the U.S. Civil Service as a Navy senior staff scientist and Esteemed Fellow of Naval Air Systems Command, Patuxent River, MD. He received a bachelor of science degree in Physics, Chemistry and Mathematics, two masters of science degrees, and a doctor of philosophy degree in Chemistry and Metallurgy from Banaras Hindu University (India) and Massachusetts Institute of Technology (USA). He has 35 years of distinguished civil service with major contributions in aircraft research and development technologies; he was awarded Department of The Navy Superior Civilian Service Medal. From 2006 - 2008, he was Associate Director at the U. S. Office of Naval Research Global - London, UK. There he served as an international agent for U.S. Navy with a mission to encourage international collaboration in Science and Technology through priority R&D in support of U.S. Naval forces.

George Vachtsevanos is a Professor Emeritus of Electrical and Computer Engineering at the Georgia Institute of Technology. He was awarded a B.E.E. degree from the City College of New York in 1962, a M.E.E. degree from New York University in 1963 and the Ph.D. degree in Electrical Engineering from the City University of New York in 1970. He directs the Intelligent Control Systems laboratory at the Georgia Institute of Technology where faculty and students are conducting research in intelligent control, neurotechnology and cardiotechnology, fault diagnosis and prognosis of large-scale dynamical systems and control technologies for Unmanned Aerial Vehicles. His work is funded by government agencies and industry. He has published over 240 technical papers and is a senior member of IEEE. Dr. Vachtsevanos was awarded the IEEE Control Systems Magazine Outstanding Paper Award for the years 2002-2003 (with L. Wills and B. Heck). He was also awarded the 2002-2003 Georgia Tech School of Electrical and Computer Engineering Distinguished Professor Award and the 2003-2004 Georgia Institute of Technology Outstanding Interdisciplinary Activities Award.